J Nonlinear Sci (2016) 26:1789–1815
DOI 10.1007/s00332-016-9319-4

Journal of Nonlinear Science

A Genealogy of Convex Solids Via Local and Global Bifurcations of Gradient Vector Fields

Gábor Domokos[1] · Philip Holmes[2] · Zsolt Lángi[3]

Received: 22 August 2015 / Accepted: 15 June 2016 / Published online: 29 June 2016

Abstract Three-dimensional convex bodies can be classified in terms of the number and stability types of critical points on which they can balance at rest on a horizontal plane. For typical bodies, these are non-degenerate maxima, minima, and saddle points, the numbers of which provide a primary classification. Secondary and tertiary classifications use graphs to describe orbits connecting these critical points in the gradient vector field associated with each body. In previous work, it was shown that these classifications are complete in that no class is empty. Here, we construct 1- and 2-parameter families of convex bodies connecting members of adjacent primary and secondary classes and show that transitions between them can be realized by codimension 1 saddle-node and saddle–saddle (heteroclinic) bifurcations in the gradient vector fields. Our results indicate that all combinatorially possible transitions can be realized in physical shape evolution processes, e.g., by abrasion of sedimentary particles.

Communicated by Alain Goriely.

✉ Zsolt Lángi
zlangi@math.bme.hu

Gábor Domokos
domokos@iit.bme.hu

Philip Holmes
pholmes@math.princeton.edu

1 Department of Mechanics, Materials and Structures, Budapest University of Technology, Műegyetem rakpart 1-3., Budapest 1111, Hungary

2 Program in Applied and Computational Mathematics and Department of Mechanical and Aerospace Engineering, Princeton University, Princeton, NJ 08544, USA

3 Department of Geometry, Budapest University of Technology, Egry József u. 1., Budapest 1111, Hungary

Keywords Codimension 2 bifurcation · Convex body · Equilibrium · Morse–Smale complex · Pebble shape · Saddle-node bifurcation · Saddle–saddle connection

Mathematics Subject Classification 52A15 · 53A05 · 53Z05

1 Introduction

1.1 Motivation and Background

The evolution of shapes of abrading bodies, such as pebbles in river beds and on beaches, has been studied for over 70 years (e.g., Rayleigh 1942, 1944a, b; Firey 1974; Bloore 1977). Data from NASA's Curiosity Rover on Mars (Williams et al. 2013; Jerolmack 2013) have rekindled interest in the subject. In addition to classical shape indices such as axis ratios and roundness (Zingg 1935; Illenberger 1991), a recent approach considers the evolution of the number of *static equilibrium points* $N(t)$ on the surface of an abrading body, i.e., points on which the body can balance at rest on a horizontal plane (Várkonyi and Domokos 2006; Domokos et al. 2010, 2014; Domokos 2015). Unlike shape indices, which require length measurements, the integer $N(t)$ can be counted in simple experiments (Domokos et al. 2010).

Abrasion occurs primarily on a body's convex hull, so to formulate a precise and relatively simple model we restrict our analysis to convex bodies K of uniform density, with surfaces described by scalar Euclidean distance functions r_K measured from the center of mass C_K. For such bodies, static equilibria are critical points of r_K at which the gradient $\nabla r_K = 0$.

The surface ∂K of a generic convex body K can exhibit three types of non-degenerate critical points: local minima, maxima, and saddle points, which are sinks, sources and saddles of the gradient vector field $\mathbf{v} = \nabla r_K$. Let S, U, H, respectively, denote the number of each of these points. Since ∂K is a topological 2-sphere, the Poincaré–Hopf Theorem (Arnold 1998) implies that

$$S + U - H = 2. \quad (1)$$

The classification schemes introduced in Várkonyi and Domokos (2006) are based on these numbers. Specifically, the *primary class* of a generic convex body K is defined as the pair of integers $\{S, U\}$. In Várkonyi and Domokos (2006), it was shown that no primary class $\{i, j\}$ is empty and a hierarchy among these classes was defined via the *Columbus algorithm*. Using explicit truncations that remove small portions from K by slicing along convex surfaces, this algorithm generates a pair of convex bodies $K' \in \{i + 1, j\}$ and $K'' \in \{i, j + 1\}$, as shown in Fig. 1. Thus, starting from the gömböc $\{1, 1\}$ (Varkonyi and Domokos 2006), every row and column can be populated, implying that the primary classification is complete in this 'static' sense.

More refined methods exist for classifying the properties of gradient vector fields $\mathbf{v} = \nabla r_K$, including graph representations of their Morse–Smale complexes (Dong et al. 2006). The vertices of these graphs are fixed points of $\mathbf{v}$, and the edges can be either isolated heteroclinic orbits connecting saddle points, representative non-isolated

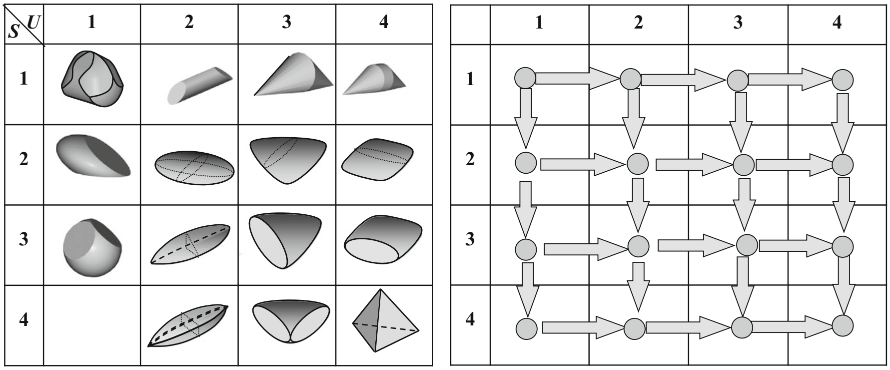

Fig. 1 Primary equilibrium classes. *Left* examples of convex bodies; *rows* and *columns* correspond to the numbers S and U of sinks and sources, respectively. *Right* the 'Columbus algorithm' of Várkonyi and Domokos (2006) defines a hierarchy among primary classes. *Arrows* indicate arbitrarily small truncations of the convex body, creating one additional sink or source and a saddle point

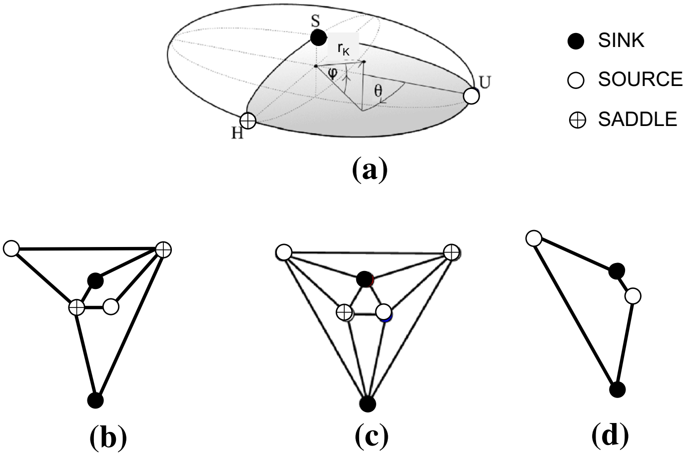

Fig. 2 Graph representations of the gradient flow on the triaxial ellipsoid in primary equilibrium class {2, 2}. **a** Distance function r_K given in spherical polar coordinates. **b** 3-colored quadrangulated primary representation $Q^3(\mathbf{v})$. **c** 3-colored triangulated representation $T^3(\mathbf{v})$. **d** Quasi-dual, 2-colored quadrangulated representation $Q^2(\mathbf{v})$. The *colors* refer to vertices, identifying them as sinks, sources, and (in **b**, **c**) saddles

heteroclinic orbits connecting saddles with sinks and sources, or both. These are called, respectively, the primary representation $Q^3(\mathbf{v})$, the triangulated representation $T^3(\mathbf{v})$, and the quasi-dual representation $Q^2(\mathbf{v})$; Fig. 2 illustrates these representations for the triaxial ellipsoid, which will be explained more thoroughly in Sect. 2. For brevity, we call all three types the *topology graphs* associated with $\mathbf{v}$. Note that all three graphs $Q^3(\mathbf{v})$, $T^3(\mathbf{v})$, and $Q^2(\mathbf{v})$ are embedded on $\mathbb{S}^2$ and we will also consider their abstract, non-embedded versions $\bar{Q}^3(\mathbf{v})$, $\bar{T}^3(\mathbf{v})$, and $\bar{Q}^2(\mathbf{v})$. We remark that an abstract graph may have several, orientation-preserving non-homeomorphic embeddings in $\mathbb{S}^2$. Precise definitions will be given in Sect. 2, and these graphs will play a key role in the paper.

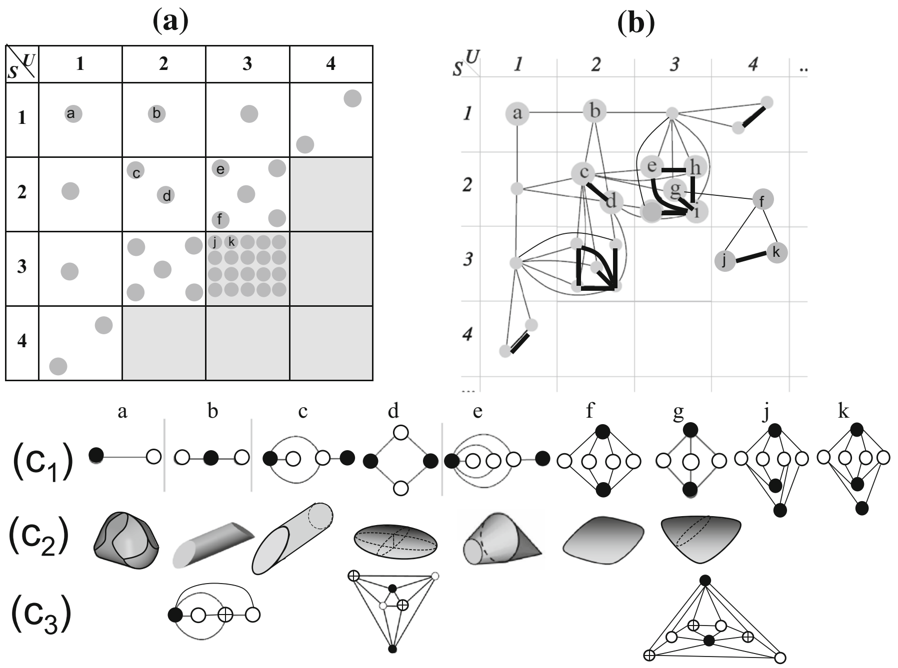

Fig. 3 Secondary and tertiary equilibrium classes. **a** Secondary and tertiary classes are contained in primary classes. **b** Metagraph $\mathcal{G}$ with vertices at tertiary classes and edges corresponding to codimension 1 bifurcations; *thin edges* saddle nodes, *thick edges* saddle–saddle bifurcations. Note that all illustrated secondary classes contain one tertiary class, so in the figure the vertices of the metagraph $\mathcal{G}$ correspond simultaneously to secondary and to tertiary classes. **c1** Quasi-dual topology graphs $Q^2(\mathbf{v})$ of the tertiary classes labeled a to k in (*a*, *b*). **c2** illustrations of a through g as convex bodies. **c3** Triangulated topology graphs $T^3(\mathbf{v})$ corresponding to *b*, *d*, and *g*

We call the class of convex bodies with isomorphic abstract graphs the *secondary equilibrium class* and the class of convex bodies with homeomorphic embedded graphs the *tertiary equilibrium class* associated with K. See Fig. 3a, which also illustrates that a primary class can contain different secondary classes: e.g., the ellipsoid is not alone in class $\{2, 2\}$; we note that even though for simplicity we illustrate topology graphs in this paper as planar maps, we always mean graphs embedded on the sphere $\mathbb{S}^2$. In Domokos et al. (2016), it was shown that the secondary and tertiary schemes are also complete in the sense that no secondary or tertiary class is empty.

One can ask whether transitions between different primary, secondary, and tertiary classes are possible within generic families $K(\lambda)$ of smooth convex bodies, parameterized by λ, as their shapes change. In generic one-parameter families of gradient vector fields, only two codimension 1 bifurcations occur: saddle nodes and saddle–saddle connections, and they do so at isolated, critical values $\lambda = \lambda_i^{cr}$ (Guckenheimer and Holmes 1983). Saddle nodes involve local changes in topology in which pairs of non-degenerate equilibria, either a saddle and a sink or a saddle and a source, emerge or disappear. Saddle–saddle bifurcations are global bifurcations at which an orbit connecting two saddle points exists, but the numbers and types of equilibria do not change.

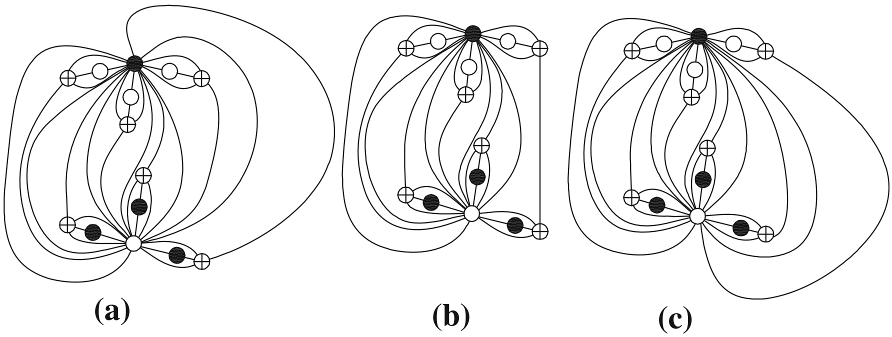

Fig. 4 Topology graphs **a** and **c** corresponding to two vertices of $\mathcal{G}$ in primary equilibrium class {4, 4} and the tertiary edge (**b**) connecting them. Graphs are shown in the triangulated representation of graph class $\mathcal{T}^3$. Note the saddle–saddle connection on (**b**), and that **a** and **c** are isomorphic as abstract graphs, but not homeomorphic as embedded graphs on $\mathbb{S}^2$

In the former, one of the integers S, U characterizing the primary class of K increases or decreases by one; in the latter, the primary class remains unchanged.

To visualize these transitions we introduce the metagraph $\mathcal{G}$ with vertices representing the embedded topology graphs associated with generic gradient fields on $\mathbb{S}^2$. The metagraph distinguishes *primary edges*, on which saddle-node bifurcations occur between vertices in different primary classes, from *secondary edges* that contain saddle–saddle bifurcations between vertices within the same primary class but in distinct secondary classes, and *tertiary edges* between vertices in the same secondary class. In Fig. 3b, primary and secondary edges are identified by thin and thick lines, respectively. Figure 3 shows only primary classes with values $S+U \leq 6$; here tertiary edges cannot be illustrated since secondary classes with so few critical points contain only one tertiary class and therefore have unique embeddings on the 2-sphere. Figure 4 illustrates a tertiary edge connecting two vertices in the primary class {4, 4}.

Our goal, which we will formally define in Sect. 1.2, is to show that not only the vertices, but also the primary and secondary edges of $\mathcal{G}$ can be represented by convex bodies, i.e., physical processes describing their shape evolution may be represented by paths on $\mathcal{G}$. It is an intriguing question which of these paths are preferred by physical abrasion processes. The investigation of this question lies beyond the scope of the current paper, but we have some physical intuition on how primary classifications of convex bodies might evolve. In Domokos (2015), it is shown that the evolution of S and U under the partial differential equations governing collisional abrasion processes can be modeled by letting S and U be random variables whose expected values decrease with time. While this trend has been verified both in laboratory experiments (Domokos et al. 2014) and in the field (Miller et al. 2014), almost no pebbles in the primary classes $\{1, i\}$, $\{j, 1\}$, $(i, j = 1, 2, \dots)$ have been found. In Domokos and Lángi (2014), a purely geometrical reason for this phenomenon was pointed out. The difficulty in reducing either the number of sinks or sources can be measured by the fraction of volume that must be removed from a solid, referred to as *robustness*. In Domokos and Lángi (2014), it was shown that the robustness of classes $\{2, i\}$, $\{j, 2\}$ is maximal so it is very unlikely that any natural pebble in these classes will be transformed into any of the classes $\{1, i\}$, $\{j, 1\}$ by natural abrasion.

Much less is known about the secondary, let alone tertiary classification of convex bodies, and theories for their evolution by abrasion are lacking. Nevertheless, as for the primary case, field data indicate that natural shapes strongly prefer some secondary classes while other classes remain virtually empty. Already in Hilbert and Cohn-Vossen (1952), it was observed that coastal pebbles tend to be ellipsoidal. While Rayleigh (1942, 1944a, b), Bloore (1977) and Firey (1974) ultimately showed that the classical *exact* ellipsoid is not an attracting state in collisional abrasion processes, nearly ellipsoidal shapes nonetheless dominate pebble beaches. Without exception, all those shapes in primary class {2, 2} for which the secondary classes were determined have topology graph ‘d’ of Fig. 3c, while the other secondary class ‘c’ in {2, 2} appears to be missing. Similar observations apply to other primary classes.

As a first step toward understanding these phenomena, we show that the secondary classification scheme of Domokos et al. (2016) is also complete in the following ‘dynamical’ sense. Primary and secondary edges in the metagraph $\mathcal{G}$, containing codimension 1 saddle node and saddle–saddle bifurcations, respectively, exist in the space of gradient vector fields $\mathbf{v} = \nabla r_K$ on the 2-sphere associated with convex bodies K. In the next subsection, we use the metagraph $\mathcal{G}$ to formulate our statements and relate them to earlier results. Before doing so, we note that the gradient vector field $\mathbf{v} = \nabla r_K$ cannot describe the Newtonian dynamics of the body K rocking on a horizontal plane, which would require a system of second-order differential equations, but that the stability types of its fixed points correctly reflect those of the equilibria of K.

1.2 Definitions and Main Result

We first define the metagraph $\mathcal{G}$, whose vertices are embedded topology graphs representing tertiary equilibrium classes associated with the Morse–Smale complexes (Milnor 1963) of gradient vector fields of convex bodies. For simplicity, we use the primary representation $Q^3(\mathbf{v})$, but the triangulated or quasi-dual representations may also be used to construct $\mathcal{G}$. The edges of $\mathcal{G}$ correspond to codimension 1 bifurcations connecting these classes, and all possible one-parameter families of gradient vector fields on the 2-sphere appear in $\mathcal{G}$. We define the edges and vertices of $\mathcal{G}$, and we will use these concepts to formulate our results and relate them to earlier results.

Definition 1 Two vector fields $\mathbf{v}$ and $\mathbf{w}$ on the 2-sphere are *topologically equivalent* (Sotomayor 1968; Guckenheimer and Holmes 1983) if there is an orientation-preserving homeomorphism of the sphere $\mathbb{S}^2$ that maps the topology graph of $\mathbf{v}$ into the topology graph of $\mathbf{w}$ for any of the types Q^3, T^3, and Q^2. We note that the existence of such homeomorphism for any of the three representations implies the existence of such a homeomorphism for each of the types.

As noted earlier, in case of generic vector fields (Sotomayor 1968), topology graphs can be defined by the Morse–Smale complex associated with the vector field (Dong et al. 2006). Now we proceed to define the metagraph $\mathcal{G}$.

Definition 2 A vertex of $\mathcal{G}$ is an embedded topology graph $Q^3(\mathbf{v})$ on $\mathbb{S}^2$, associated with the Morse–Smale complex of a generic gradient vector field $\mathbf{v}$ on $\mathbb{S}^2$.

Definition 3 The primary class of a vertex $Q^3(\mathbf{v})$ is the pair of integers $\{S, U\}$, where S and U denote the number of sinks and saddles of $\mathbf{v}$. The secondary and tertiary class of a vertex are the abstract graph $\bar{Q}^3(\mathbf{v})$ and the embedded graph $Q^3(\mathbf{v})$, respectively, both associated with the Morse–Smale complex of $\mathbf{v}$.

Definition 4 An edge of $\mathcal{G}$ is a one-parameter family $\mathbf{v}(\lambda), \lambda \in [0, 1]$ of gradient vector fields connecting two distinct vertices $Q^3(\mathbf{v}(0))$ and $Q^3(\mathbf{v}(1))$ of $\mathcal{G}$. We require that $\mathbf{v}$ is generic except for a unique value $\lambda = \lambda^\star \in (0, 1)$, for which $\mathbf{v}(\lambda^\star)$ exhibits a codimension 1 bifurcation (Guckenheimer and Holmes 1983).

Definition 5 We call an edge $\mathbf{v}(\lambda), \lambda \in [0, 1]$ primary if the primary classes of $Q^3(\mathbf{v}(0))$ and $Q^3(\mathbf{v}(1))$ are different. We call an edge $\mathbf{v}(\lambda), \lambda \in [0, 1]$ secondary if the primary class of $Q^3(\mathbf{v}(0))$ and $Q^3(\mathbf{v}(1))$ are identical, but their secondary classes are different. We call an edge $\mathbf{v}(\lambda), \lambda \in [0, 1]$ tertiary if both the primary and the secondary class of $Q^3(\mathbf{v}(0))$ and $Q^3(\mathbf{v}(1))$ are identical.

Definition 6 We call a vertex $Q^3(\mathbf{v})$ of $\mathcal{G}$ physical if there exists a convex body K such that ∇r_K is topologically equivalent to $\mathbf{v}$.

Definition 7 We call a primary, secondary or tertiary equilibrium class physical if it contains at least one physical vertex.

Definition 8 We call an edge $\mathbf{v}(\lambda), \lambda \in [0, 1]$ of $\mathcal{G}$ physical if there exists a one-parameter family $K(\lambda), \lambda \in [0, 1]$ of convex bodies such that $\nabla r_K(\lambda)$ is topologically equivalent to $\mathbf{v}(\lambda)$ for all values of $\lambda \in [0, 1]$.

Now we can formulate earlier and current results. Regarding primary equilibrium classes, we have

Theorem 1 *All primary classes are physical.*

This result, proved in Várkonyi and Domokos (2006), was generalized in Domokos et al. (2016) to include secondary and tertiary classes:

Theorem 2 *All vertices of $\mathcal{G}$ are physical.*

In the current paper, our goal is to further extend Theorems 1 and 2 by proving the physical existence of an important subset of edges of $\mathcal{G}$:

Theorem 3 *All primary and secondary edges of $\mathcal{G}$ are physical.*

1.3 Summary of Proof

As noted above, the local truncations constructed in Domokos et al. (2016) modify the Morse–Smale complex of K to produce one-parameter families of convex bodies in which either S or U is increased by 1. However, these families do not (necessarily) represent edges in the metagraph $\mathcal{G}$ since the genericity of the bifurcation was not guaranteed by the construction in Domokos et al. (2016). One-parameter families connecting vertices at the ends of secondary edges (saddle–saddle connection bifurcations) were not even discussed in Domokos et al. (2016).

Here, we extend these results by constructing a 2-parameter family of convex bodies whose gradient vector fields are generic in the sense that certain codimension 1 subsets (curves) in the parameter plane correspond to vector fields with codimension 1 local saddle-node and global saddle–saddle bifurcations, forming primary and secondary edges of $\mathcal{G}$. We also show that the codimension 1 bifurcation curves meet in a codimension 2 saddle to saddle-node bifurcation point.

Because secondary edges correspond to codimension 1 global saddle–saddle bifurcations, the local methods of Domokos et al. (2016) do not apply directly. Rather, we achieve our goal in two steps. In Sect. 2, we prove Combinatorial Lemma 1, stating that any secondary edge of the metagraph $\mathcal{G}$ bounds a triangular face of $\mathcal{G}$ of which the two other edges are primary. As shown in Fig. 9 below, the vertices of such a face represent three topology graphs that lie in adjacent primary classes of $\mathcal{G}$. The triangles (b,c,d) and (f,j,k) in Fig. 3b above provide examples. We then appeal to dynamical systems theory (Guckenheimer and Holmes 1983) in Sect. 3 to show that such a triangular face could contain a codimension 2 bifurcation point for the gradient flow $\mathbf{v} = \nabla r_{K(\lambda)}$ and describe how codimension 1 saddle-node and saddle–saddle bifurcations emanate from this point.

In Sect. 4, we take the second step, providing an explicit geometrical construction that realizes the codimension 2 bifurcation via an arbitrarily small truncation of K depending on two parameters. First, in Sect. 4.1 we prove that a truncation exists under the assumption that the resulting displacement of the body's mass center has no effect on the topology of its gradient flow. Then, in Sect. 4.2 we construct a *simultaneous*, auxiliary truncation such that the mass center remains fixed under the combined truncations, implying that the topology of the flow is preserved. Finally, in Sect. 5 we summarize our results and point out some possible consequences.

2 Combinatorial Part

Before stating the combinatorial lemma, we define three classes of graphs associated with Morse–Smale complexes on the 2-sphere, of which the graph representations introduced above and illustrated in Fig. 2b–d are examples. As in Domokos et al. (2016), we denote by a *quadrangulation* a finite planar undirected multigraph on the 2-sphere in which each face is bounded by a closed walk of length 4 (cf. Archdeacon et al. 2001; Brinkmann et al. 2005). A multigraph contains no loops but may have multiple (parallel) edges, and it is usually permitted that the boundary of a face may contain a vertex or an edge of the graph more than once (e.g., see some of the faces with saddle–source and source–sink connections in Fig. 5a, c, respectively). In addition, we follow (Archdeacon et al. 2001) and regard the *path graphs* (cf. Gross and Yellen 2006) P_2 and P_3 as quadrangulations, where P_k denotes a tree on k vertices, each with degree at most 2.

Dong et al. (2006) introduced three different kinds of graph to represent a Morse–Smale complex on the 2-sphere, as follows:

- $\mathcal{Q}^2$ is the class of 2-vertex-colored quadrangulations. Note that as no quadrangulation contains odd cycles, each is 2-colorable (cf. Archdeacon et al. 2001; Nakamoto 1999). Furthermore, the coloring of the graph is unique up to switching the colors.

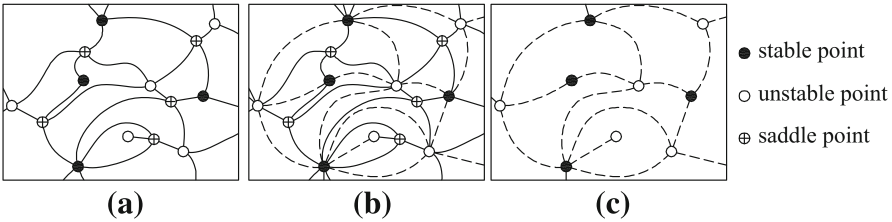

Fig. 5 Different representations of a part of a Morse–Smale complex. **a** Primary topology graph in class $\mathcal{Q}^3$. **b** Triangulated topology graph in class $\mathcal{T}^3$. **c** Quasi-dual topology graph in class $\mathcal{Q}^2$

- $\mathcal{Q}^3$ is the class of 3-vertex-colored quadrangulations with $\deg(p) = 4$ for any $p \in H$, and $|\mathcal{S}| + |\mathcal{U}| - |\mathcal{H}| = 2$, where $\mathcal{S}, \mathcal{U}$, and $\mathcal{H}$ denote the sets of vertices of each given color.
- $\mathcal{T}^3$ is the class of 3-vertex-colored triangulations with $\deg(p) = 4$ for any $p \in \mathcal{H}$, and $|\mathcal{S}| + |\mathcal{U}| - |\mathcal{H}| = 2$, where $\mathcal{S}, \mathcal{U}$, and $\mathcal{H}$ denote the sets of vertices of each given color.

Examples of each class appear in Fig. 5c, a, b, respectively.

It was shown in Edelsbrunner et al. (2003) (cf. Zomorodian 2005) that a Morse–Smale complex on the 2-sphere can be uniquely represented by a 3-vertex-colored quadrangulation in $\mathcal{Q}^3$, where the vertex colors represent the 3 types of critical points (maxima, minima, and saddles) and edges correspond to stable and unstable manifolds: isolated integral curves that end and start at saddle points. Each quadrangle is bounded by a closed walk consisting of a source, a saddle, a sink and a saddle in cyclic order around the face, and every saddle has degree 4; see Fig. 5a. Following Dong et al. (2006), we call this the *primary* topology graph.

Saddle points can be removed from the primary graph without losing information (Dong et al. 2006): first we connect sources and sinks inside each quadrangle, producing a *triangulated* topology graph in class $\mathcal{T}^3$; we then remove all saddle points and edges incident to them, as in Fig. 5b, c. Since non-degenerate saddles have degree 4, the resulting graph is a 2-vertex-colored quadrangulation in class $\mathcal{Q}^2$: the *quasi-dual* topology graph (cf. Dong et al. 2006). Here, we use the latter; however, in Sect. 4, the primary graph representation is preferable. All three representations are equivalent in the sense that they are mutually uniquely identified.

Let $F = (p_1, p_2, p_3, p_4)$ be a face of any $Q \in \mathcal{Q}^2$ (cf. Fig. 6a1, left). Pairs of vertices, and/or edges connecting them, may coincide. Nonetheless, a quasi-dual representation admits only two kinds of coincidences: two diagonally opposite vertices, say p_2 and p_4 may coincide, and in this case two consecutive edges, say (p_4, p_1) and (p_1, p_2) may coincide: these two cases are illustrated in Fig. 6b1, c1, left. Note that in Fig. 6c1 the internal domain bordered by the edges (p_4, p_1) and (p_1, p_2) is not a quadrangular face and necessarily contains at least one additional vertex, as indicated by the triangles in the inner region. Figure 6d1 shows the remaining two exceptional cases: the trees $Q = P_3$ and $Q = P_2$.

The algorithm in Domokos et al. (2016) is based on repeated application of a combinatorial graph operation called *face contraction* (cf. Archdeacon et al. 2001; Brinkmann et al. 2005 or Negami and Nakamoto 1993). Applied to the face F defined

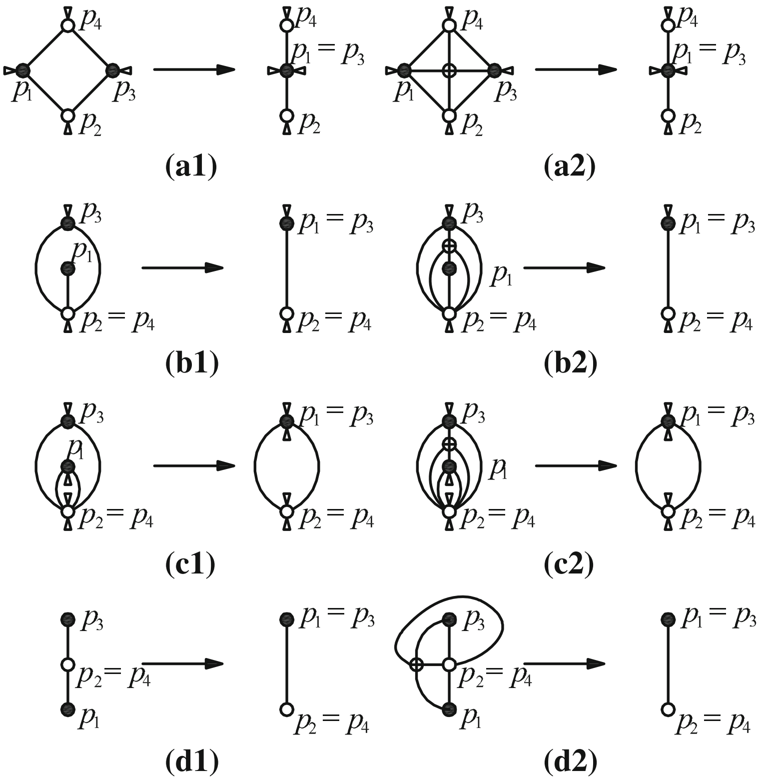

Fig. 6 **a1–d1** Face contractions on the subgraph of a graph in class $\mathcal{Q}^2$. As in Brinkmann et al. (2005), *triangles* incident to some vertices indicate that one or more edges *may* occur at that position around the vertex. Here p_1 and p_3 are sinks; analogous face contractions, each removing a source from the graph, can be performed by switching the colors. **a2–d2** The corresponding face contractions in class $\mathcal{T}^3$

in the previous paragraph, this operation results in the contraction of the vertices p_1 and p_3 into the same vertex, and the disappearance of F; the modified graphs depending on the 'shape' of the original face F are shown on the right of each panel in Fig. 6. The inverse operation of face contractions is called *vertex splitting*. Combinatorially, for graphs with at least three vertices it can be defined as follows. Let p be a vertex of the quadrangulation Q, with adjacent edges $E_1, E_2, \ldots, E_k, E_{k+1} = E_1$ in counterclockwise order, and note that the other endpoints of some of these edges may coincide. Choose two, not necessarily distinct edges: E_x and E_y. Then, we split p into two vertices p_1 and p_3, and E_x and E_y into two pairs of edges $E_{x,1}$ and $E_{x,3}$, and $E_{y,1}$ and $E_{y,3}$, such that $E_{x,1}, E_{x+1}, \ldots, E_{y-1}, E_{y,1}$ are connected to p_1, and $E_{y,3}, E_{y+1}, \ldots, E_{x-1}$ and $E_{x,3}$ are connected to p_3. This operation can be naturally modified for primary and triangulated representations: in the primary representation, instead of two edges we choose two (not necessarily distinct) faces, whereas in a triangulated representation we choose two edges connecting a sink and a source.

In a quasi-dual graph, a transition via a saddle–saddle connection can be realized as a *diagonal slide* (Negami and Nakamoto 1993), defined as follows: consider two faces

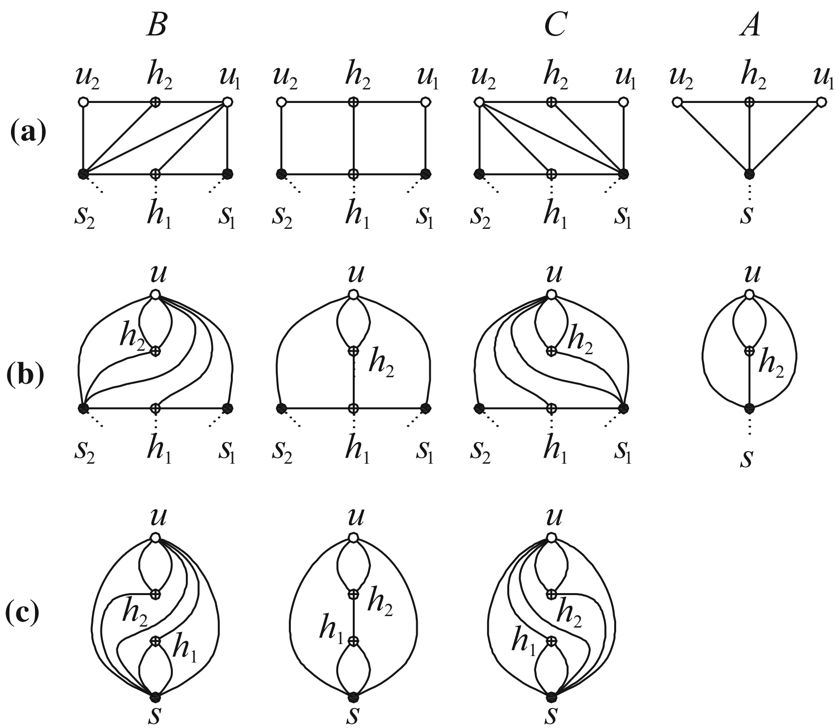

Fig. 7 The connection between diagonal slides and twin vertex splittings for subgraphs of $\mathcal{T}^3$-class graphs. Row (*a*) the non-degenerate case. Row (*b*) the degenerate case when $u_1 = u_2$, labeled by u. Row (*c*) the degenerate case when $u_1 = u_2 = u$ and $s_1 = s_2 = s$. The subgraphs in row (*c*), columns *B* and *C* belong to isomorphic graphs, and thus have no common ancestor, hence no subgraph appears in column *A* of row (*c*)

(s_1, u_3, s_2, u_2) and (u_1, s_3, u_2, s_2) of the quadrangulation sharing an edge (s_2, u_2), and replace this edge by either (s_1, u_1) or (s_3, u_3), say (s_3, u_3). Then, the two faces (s_1, u_3, s_2, u_2) and (u_1, s_3, u_2, s_2) are replaced by (s_1, u_3, s_3, u_2) and (u_1, s_3, u_3, s_2). To formulate the lemma, we need the following definition.

Definition 9 Let $Q \in \mathcal{Q}^2$ be a quadrangulation. Two vertex splittings W and W' of Q are called *twin*, if:

- The same vertex p is split.
- Let A_1 and A_2 denote the sets of edges connected to the two split vertices in W, and define A'_1 and A'_2 similarly for W'. Then, A_1 differs in exactly one element from A'_1 or A'_2.

In this case, Q is called the *ancestor* of the two split graphs. This definition can also be naturally interpreted for primary and triangulated representations.

Note that the second property in Definition 9 implies that A_2 also differs in exactly one element from A'_1 or A'_2. The graphs in columns B and C of rows (a) and (b) in Fig. 7 can be obtained from the graph in column A of the same row via twin vertex splittings, but the graphs in columns B and C of Fig. 7c are isomorphic and hence have no ancestor graph. This corresponds to the degenerate case 3 in the Proof of the Combinatorial Lemma 1 below.

Lemma 1 *(*Combinatorial Lemma*) Let $B, C \in \mathcal{Q}^2$ be embeddings of two non-isomorphic abstract graphs $\bar{B}, \bar{C}$ in $\mathbb{S}^2$, respectively, such that there is a diagonal slide that transforms B into C. Then there is an embedding $A \in \mathcal{Q}^2$ and a pair of* twin *vertex splittings W_B and W_C of $\bar{A}$ such that W_B transforms A into B, and W_C transforms A into C.*

We remark that, as we will see in the proof of Lemma 1, there are diagonal slides between non-homeomorphic drawings of the same graph which cannot be derived from the same ancestor via twin vertex splittings. Note also the essential condition that the abstract graphs $\bar{B}, \bar{C}$ should be non-isomorphic; this condition excludes tertiary edges from our argument.

Proof To simplify the proof, we use the triangulated variants of B and C, which with a little abuse of notation, we also denote by B and C. Let the two saddles that are connected by the saddle–saddle bifurcation be denoted by h_1 and h_2. This edge belongs to two faces of B, say (s_2, u_1, h_1) and (s_2, u_1, h_2), and similarly, two faces of C, say (s_1, u_2, h_1) and (s_1, u_2, h_2). We note that, due to the degeneracy of the graph, some of the vertices or edges may coincide; nevertheless, due to the saddle–saddle connection, h_1 and h_2 are distinct.

Case 1 s_1 and s_2, and also u_1 and u_2 are distinct. Figure 7 row (a) shows the corresponding faces of B, the saddle–saddle bifurcation, C, and the common ancestor A from left to right. Face contractions are carried out by collapsing the edges (s_1, h_1) and (s_2, h_1) into a single vertex s, and the dotted edges starting at s_1, h_1 and s_2 are contracted into the single dotted edge of A. Furthermore, the edges (s_2, u_1), (h_1, u_1), and (s_1, u_1) are contracted to (s, u_1) in B, whereas (s_2, u_2), (h_1, u_2) and (s_1, u_2) are contracted to (s, u_2) in C. Since (s, u_1) and (s, u_2) are consecutive edges of A in the quasi-dual representation, the vertex splittings belonging to the two face contractions are indeed twin. We remark that in Case 1 (row a) another ancestor can be found by contracting (u_1, h_2) and (u_2, h_2).

Case 2 exactly one of the pairs $\{s_1, s_2\}$ or $\{u_1, u_2\}$ coincide. Without loss of generality, we may assume that $u_1 = u_2 = u$ and $s_1 \neq s_2$. Note that as the degree of a saddle point is 4, in this case there are two edges starting at h_2 and ending at u. Figure 7 row (b) shows the corresponding faces of B, the saddle–saddle bifurcation, C, and the common ancestor A from left to right. Face contraction is carried out by collapsing the edges (s_1, h_1) and (s_2, h_1) into a single vertex s.

Case 3 $s_1 = s_2 = s$, and $u_1 = u_2 = u$. In this case, B and C are isomorphic graphs: Fig. 7 row (c). We note that in this case the two edges starting at s and ending at u may also coincide. □

3 Dynamical Part

In this section, we describe how codimension 1 saddle-node and saddle–saddle bifurcations can meet in a codimension 2 bifurcation of a gradient vector field $\mathbf{v}$ on $\mathbb{S}^2$. Such a bifurcation point can be associated with each triangular face of the metagraph $\mathcal{G}$ having two primary edges and one secondary edge. We construct an explicit polynomial function $V_{\mu_1,\mu_2}(x, y)$, depending on two parameters μ_1, μ_2, that captures the behavior of **v** near a degenerate saddle node whose strong stable manifold contains one branch of the unstable manifold of a non-degenerate (hyperbolic) saddle point. The parameters μ_1, μ_2 provide local coordinates on the face of the metagraph near the codimension 2 point. Since the saddle–saddle or *heteroclinic* connection is a global phenomenon, our vector field will necessarily be non-local, but we can nonetheless find a cubic potential function that captures the local saddle-node and the global heteroclinic connection. A *homoclinic* orbit to a saddle-node bifurcation point was previously shown to occur in the averaged equations for the periodically forced van der Pol oscillator (Holmes and Rand 1978), cf. (Guckenheimer and Holmes 1983, Sect. 2.1, Figs. 2.1.2-3).

We first recall the normal form of an isolated codimension 1 saddle node in a gradient vector field on the plane, which can be described by a potential function depending on one parameter (Guckenheimer and Holmes 1983):

$$V_{\mu_1}(x, y) = \frac{x^3}{3} + \frac{y^2}{2} - \mu_1 x, \tag{2}$$

The corresponding vector field

$$\begin{aligned} \dot{x} &= -\frac{\partial V_{\mu_1}}{\partial x} = -x^2 + \mu_1, \\ \dot{y} &= -\frac{\partial V_{\mu_1}}{\partial y} = -y, \end{aligned} \tag{3}$$

has no fixed points for $\mu_1 < 0$, a saddle node at $(x, y) = (0, 0)$ for $\mu_1 = 0$, and a hyperbolic saddle and a sink at $(x, y) = (-\sqrt{\mu_1}, 0)$ and $(+\sqrt{\mu_1}, 0)$, respectively, for $\mu_1 > 0$.

We now add further cubic terms and a linear term containing another parameter μ_2 to V_{μ_1} to produce a second hyperbolic saddle that can be displaced relative to the saddle and sink described above. We set

$$V_{\mu_1,\mu_2,\alpha}(x, y) = \frac{x^3}{3} + \frac{y^2}{2} + \frac{y^3}{3} - \alpha x^2 y - \mu_1 x - \mu_2 xy, \text{ with } \alpha \geq (1/4)^{1/3}, \tag{4}$$

so that the vector field (3) becomes

$$\begin{aligned} \dot{x} &= -x^2 + 2\alpha xy + \mu_1 + \mu_2 y, \\ \dot{y} &= \alpha x^2 - y - y^2 + \mu_2 x. \end{aligned} \tag{5}$$

Elementary calculations and linearization at the fixed points show that, for $\mu_1 = \mu_2 = 0$, the saddle node remains at $(0, 0)$ and a hyperbolic saddle lies at $(0, -1)$. Moreover, the y-axis is an invariant line, because $\dot{x} \equiv 0$ for any solution with initial condition $(0, y_0)$. The unstable manifold of the saddle $(0, -1)$ is the line segment $\{x = 0 | y \in (-\infty, 0)\}$, the upper part of which coincides with the lower part of the

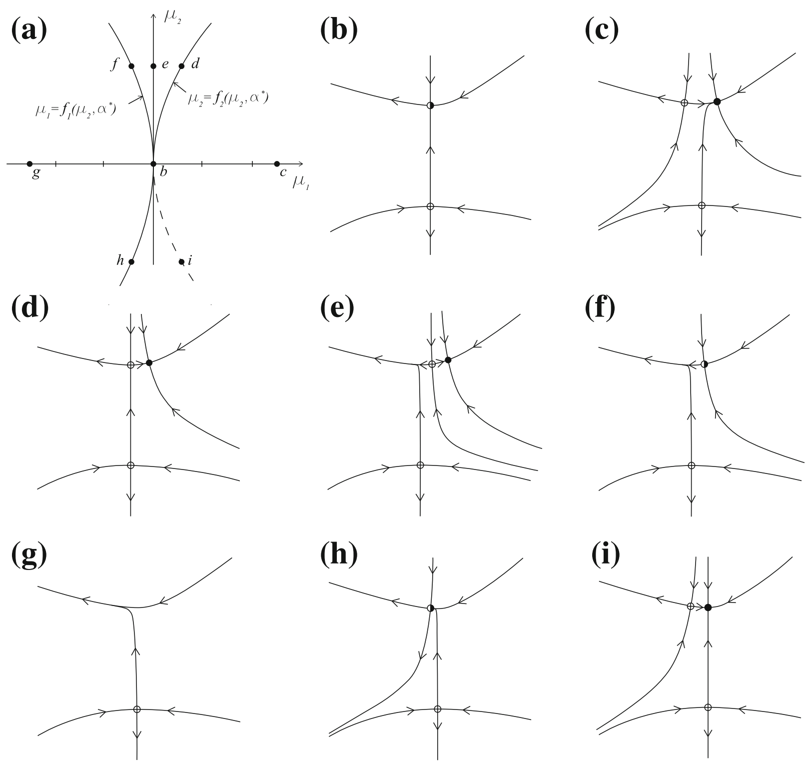

Fig. 8 Bifurcations of the gradient vector field (5). **a** The bifurcation set in (μ_1, μ_2)-space near the codimension 2 point (0, 0): saddle nodes occur on the curve $\mu_1 = f_1(\mu_2; \alpha) \neq 0$; saddle–saddle connections exist on the curve $\mu_1 = f_2(\mu_2; \alpha) = \left\{\mu_2^2/4\alpha^2 | \mu_2 \in (0, \sqrt{\alpha})\right\}$. **b** At $\mu_1 = \mu_2 = 0$ the unstable manifold of the saddle at $(0, -1)$ lies in the strong stable manifold of the saddle node at (0, 0). **c** For $\mu_1 > \max\{f_1(\mu_2; \alpha), f_2(\mu_2; \alpha)\}$ two unconnected hyperbolic saddles coexist with a sink. **d** Along $\mu_1 = f_2(\mu_2; \alpha) < \alpha^2$ with $\mu_2 > 0$ a codimension 1 saddle–saddle connection exists on the invariant line $x = -\sqrt{\mu_1}$. **e** For $f_1(\mu_2; \alpha) < \mu_1 < f_2(\mu_2; \alpha)$ and $\mu_2 > 0$ two hyperbolic saddles and a sink exist with the lower saddle's unstable manifold passing left of the upper saddle's stable manifold. **f** On $\mu_1 = f_1(\mu_2; \alpha) < 0$ with $\mu_2 > 0$ a codimension 1 saddle node occurs with the lower saddle's unstable manifold passing to its left. **g** For $\mu_1 < f_1(\mu_2; \alpha)$ only the lower saddle exists. **h** On $\mu_1 = f_1(\mu_2; \alpha) < 0$ with $\mu_2 < 0$ a codimension 1 saddle node occurs with the lower saddle's unstable manifold entering from its right. **i** Along $\mu_1 = f_2(\mu_2; \alpha)$ with $\mu_2 < 0$ the lower saddle's unstable manifold lies on the invariant line $x = +\sqrt{\mu_1}$ and intersects the strong stable manifold of the sink; this is *not a bifurcation point*

strong stable manifold $\{x = 0 | y \in (-1, +\infty)\}$ of the saddle node. A disk containing these two fixed points constitutes a chart, containing the codimension 2 degenerate vector field that can be mapped onto an open set of $\mathbb{S}^2$: see Fig. 8b. The term $-\alpha x^2 y$ is necessary to make the lower saddle hyperbolic (its eigenvalues are -2α and $+1$). A second hyperbolic saddle lies at $(2\alpha/(4\alpha^3 - 1), 1/(4\alpha^3 - 1)$, but this fixed point is irrelevant to the bifurcations of interest, and it can be driven out of any compact region by letting $\alpha \to (1/4)^{1/3} \stackrel{\text{def}}{=} \alpha^* \approx 0.62996$. For the cases shown in Fig. 8b–j we set $\alpha = 0.62996$.

We now describe the codimension 1 bifurcations and structurally stable vector fields that emerge from the codimension 2 bifurcation point for small μ_1, μ_2. Setting $\dot{x} = \dot{y} = 0$ in (5), and noting that $y = (x^2 - \mu_1)/(2\alpha x + \mu_2)$ from the first equation, we may eliminate y from the second equation to obtain the fixed point condition

$$F_{\mu_1,\mu_2,\alpha}(x) = a_4 x^4 + a_3 x^3 + a_2 x^2 + a_1 x + a_0 = 0, \tag{6}$$

where

$$a_4 = 4\alpha^3 - 1, a_3 = 2\alpha(4\alpha\mu_2 - 1), a_2 = 2\mu_1 + 5\alpha\mu_2^2 - \mu_2,$$
$$a_1 = 2\alpha\mu_1 + \mu_2^3 \text{ and } a_0 = \mu_1\mu_2 - \mu_1^2. \tag{7}$$

For $\mu_1 = \mu_2 = 0$ Eqn. (6) becomes $((4\alpha^3 - 1)x - 2\alpha)x^3 = 0$, with a triply degenerate root at $x = 0$ and the irrelevant root at $x = 2\alpha/(4\alpha^3 - 1)$. Setting $\alpha = \alpha^*$ so that the latter root lies at ∞, the quartic polynomial becomes a cubic with discriminant

$$\Delta = 18a_0a_1a_2a_3 - 4a_0a_2^3 + a_1^2a_2^2 - 4a_1^3a_3 - 27a_0^2a_3^2. \tag{8}$$

To obtain an explicit approximation for the saddle-node bifurcation curve $\mu_1 = f_1(\mu_2; \alpha^*)$, we consider this special case. Substituting the expressions (7) into (8) and setting $\Delta = 0$ yields a polynomial relating μ_1 and μ_2 for which $F_{\mu_1,\mu_2,\alpha^*}(x_0) = F'_{\mu_1,\mu_2,\alpha^*}(x_0) = 0$ and one of relevant roots x_0 is multiple. Except for $\mu_1 = \mu_2 = 0$, for which $x_0 = 0$ and $F''_{\mu_1,\mu_2,\alpha^*}(0) = 0$, this is a double root, and it corresponds either to a saddle-node bifurcation, or to the heteroclinic saddle–saddle connection discussed below. Expanding μ_1 in integer powers of μ_2 and using the fact that $a_3 = -2\alpha + \mathcal{O}(\mu_2)$ to determine the leading terms, we find the following expression for the saddle-node bifurcation:

$$\mu_1 = f_1(\mu_2; \alpha^*) = -\frac{\mu_2^4}{4} - \frac{3 \times 2^{1/3}\mu_2^5}{8} - \frac{5 \times 2^{2/3}\mu_2^6}{8} + \mathcal{O}\left(\mu_2^7\right). \tag{9}$$

As in Eqn. (3), μ_1 primarily controls the saddle-node bifurcation, but the second parameter μ_2 shifts the relative x positions of the upper and lower saddles, allowing a codimension 1 heteroclinic connection to form with $\mu_1 \neq 0$. Specifically, along the curve

$$\mu_1 = f_2(\mu_2; \alpha) = \frac{\mu_2^2}{4\alpha^2}, \quad \text{with } \mu_2 \in (0, \sqrt{\alpha}), \tag{10}$$

both saddle points lie on the invariant line $x = -\sqrt{\mu_1}$ and a connecting orbit from the lower to the upper saddle exists (their y coordinates are $\frac{1}{2}\left[-1 \mp \sqrt{1 - \mu_2^2/\alpha}\right]$, respectively). This bifurcation curve is shown in Fig. 8a for $\alpha = \alpha^*$, together with the saddle-node curve $\mu_1 = f_1(\mu_2; \alpha^*)$ (the latter's curvature is exaggerated for clarity). Note that the discriminant $\Delta = 0$ for $\mu_1 = \mu_2^2/4\alpha^{*2}$ since both saddles have the same x-coordinate. A similar invariant line $x = +\sqrt{\mu_1}$ connects the lower saddle

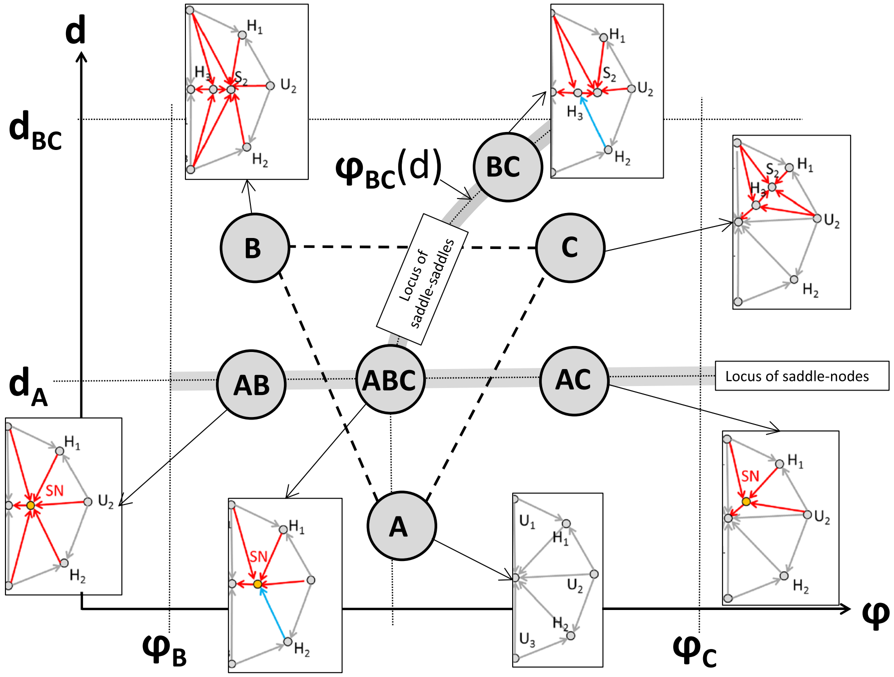

Fig. 9 A codimension 2 bifurcation on a triangular face of the metagraph $\mathcal{G}$. For better comparison with other figures, all topology graphs are shown in the triangulated $\mathcal{T}^3$ representation, however, observe that in the proof we use the primary $\mathcal{Q}^3$ representation of the same graphs. The generic graphs A, B, C can be regarded as subgraphs of a topology graph. For example, by adding one stable point, they are identical to triangulated representations of the graphs (f, j, k) in Fig. 3. The degenerate graphs AB, AC, containing codimension 1 saddle-node bifurcations SN, correspond to primary edges fj, fk of $\mathcal{G}$. The degenerate graph BC containing a codimension 1 saddle–saddle connection H2-H3 corresponds to the secondary edge jk of the metagraph. Finally, the degenerate graph ABC, containing the codimension 2 bifurcation, corresponds to the triangular face fjk of the metagraph $\mathcal{G}$

to the strong stable manifold of the sink for $\mu_1 = \mu_2^2/4\alpha^2$ with $\mu_2 < 0$, but since saddle–sink connections are structurally stable, no bifurcation occurs here (Fig. 8j).

In addition to the degenerate codimension 2 vector field at $(\mu_1, \mu_2) = (0, 0)$ shown in panel (b), panels (c–h) show representative vector fields on the codimension 1 bifurcation curves and structurally stable vector fields in the three open regions in the bifurcation set of panel (a). For the unfolding parameters used here, the saddle-node and saddle–saddle connection bifurcation curves meet in a quadratic tangency at $(\mu_1, \mu_2) = (0, 0)$. The geometrical parameters (d, ϕ) chosen in the construction that follows produce bifurcation curves that meet transversely at $(0, 0)$, as shown in Fig. 9.

4 Geometrical Part

In this section, we prove Theorem 3. To do this, it suffices to create for any primary or secondary edge $E = \{v_1, v_2\}$ of the metagraph $\mathcal{G}$ a *suitable,* one-parameter family

$K(\lambda)$ of convex bodies, where $\lambda \in [\lambda_1, \lambda_2]$, with a unique value $\lambda^\star \in (\lambda_1, \lambda_2)$ such that the graph of $K(\lambda)$ is homeomorphic to v_1 for any $\lambda \in [\lambda_1, \lambda^\star)$, homeomorphic to v_2 for any $\lambda \in (\lambda^\star, \lambda_2]$, and homeomorphic to the graph of the codimension-1 bifurcation defined by $E = \{v_1, v_2\}$ at $\lambda = \lambda^\star$. In this case we can choose a re-parameterization of this family that will satisfy the topological equivalence condition of the theorem. For simplicity, when in the proof we write about homeomorphic topology graphs, we mean that there is an orientation-preserving homeomorphism mapping one embedding into the other one.

We prove the assertion only for secondary edges of $\mathcal{G}$, because for primary edges we may apply a simpler version of the same argument. As noted before, our argument does not apply to tertiary edges. Secondary edges correspond to non-local bifurcations, so it is hard to construct by local truncations a suitable one-parameter family of convex bodies that corresponds to any given secondary edge. To ensure that local truncations suffice, we rely on Lemma 1, stating that any secondary edge belongs to a triangular face of $\mathcal{G}$ of which the two other edges are primary. Since the latter correspond to local saddle-node bifurcations, we can use local truncations. We will show that any face of $\mathcal{G}$ spanned by two primary edges and one secondary edge can be realized by a *suitable* 2-parameter family $K(d, \phi)$ of convex bodies (cf. Definition 10). Such a family has (among others) the property that it collapses to family described above if we restrict to any of the three edges of $\mathcal{G}$, so the existence of this suitable 2-parameter family proves the Theorem.

Let B and C be the primary graph representations of two gradient vector fields that are connected via any given saddle–saddle bifurcation. Furthermore, let A be their common ancestor, that is, B and C can be derived from A by twin vertex splittings. By Lemma 1, such a graph exists and from Domokos et al. (2016) we know that each of the three graphs A, B, C can be associated with the gradient vector fields of the smooth, convex bodies K_A, K_B, K_C, respectively. We denote the degenerate graphs belonging to the corresponding transitions by AB, AC, BC, and ABC, respectively. See Fig. 9.

Definition 10 A 2-parameter family $K(d, \phi)$ of convex bodies, where $d \in [0, d_{BC}]$ and $\phi \in [\phi_B, \phi_C]$ is called *suitable* if the function $(d, \phi) \mapsto K(d, \phi)$ is continuous with respect to Hausdorff distance, and there is a value $d_A \in (0, d_{BC})$ and a function $\phi_{BC} : [d_A, d_{BC}] \in (\phi_B, \phi_C)$ such that the following holds:

(10.1) for every $\phi \in [\phi_B, \phi_C]$, $K(0, \phi) = K_A$,
(10.2) for every $\phi \in [\phi_B, \phi_C]$ and $d < d_A$, the graph of $K(d, \phi)$ is homeomorphic to A,
(10.3) for every $d > d_A$ and $\phi < \phi_{BC}(d)$, the graph of $K(d, \phi)$ is homeomorphic to B,
(10.4) for every $d > d_A$ and $\phi > \phi_{BC}(d)$, the graph of $K(d, \phi)$ is homeomorphic to C,
(10.5) for every $\phi < \phi_{BC}(d_A)$, the graph of $K(d_A, \phi)$ is homeomorphic to AB,
(10.6) for every $\phi > \phi_{BC}(d_A)$, the graph of $K(d_A, \phi)$ is homeomorphic to AC,
(10.7) for every $d > d_A$, the graph of $K(d, \phi_{BC}(d))$ is homeomorphic to BC,
(10.8) the graph of $K(d_A, \phi_{BC}(d_A))$ is homeomorphic to ABC.

We note that in Definition 10, each topology graph is taken *with respect to the center of mass of* $K(d, \phi)$, which depends on the values of d and ϕ. Nevertheless, if the same properties hold *with the center of mass of* K_A *as a fixed reference point*, we say that $K(d, \phi)$ is *weakly suitable*.

This definition is illustrated in Fig. 9. We remark that, in the context of Sect. 3, the line $\{d = d_A | \phi \in [\phi_B, \phi_C]\}$ and the curve $\{\phi = \phi_{BC}(d) | d \in [d_A, d_{BC}]\}$ form the bifurcation set associated with the gradient vector field.

We prove the assertion in two steps: in the first step (Sect. 4.1), we construct a weakly suitable family. In the second step (Sect. 4.2), we modify the construction in such a way that the center of mass of *every* member of the family coincides with that of K_A, showing that the previously constructed family is not only weakly suitable but can be made suitable.

4.1 Neglecting the Motion of the Center of Mass

In the first step of the proof, we assume that the graph of *every* convex body is taken with respect to the center of mass of K_A, i.e., we assume that the displacement of the center of mass does not influence the topology of the flow. For brevity, we set $K = K_A$, and we consider only the case that the equilibrium point of K to be split is stable; if it is unstable, a similar argument with an arbitrarily small, conical extension of the surface can be applied.

Let s denote this stable point and the descendant points in the graphs B and C, obtained by splitting s, be s'_B, s''_B, s'_C, s''_C, respectively. Appealing to Lemma 5 of Domokos et al. (2016), we may assume that a neighborhood of s in ∂K belongs to a sphere $\mathbb{S}$. Without loss of generality, let the origin o be the center of this sphere, where the radius of $\mathbb{S}$ is assumed to be one. Furthermore, let c denote the center of mass of K, and note that, because s is a stable point, c is contained in the interior of the segment $[o, s]$ (cf. Fig. 10b).

Let Γ_i, where $i = 1, 2, \dots, m$ denote the edges of A starting at s, in counterclockwise order around s, from outside K. Clearly, for each value of i, the part of Γ_i in $\mathbb{S}$ is a great circle arc. These edges are labeled in such a way that the edges of B starting at s'_B correspond to the Γ_i's with $i = 1, 2, \dots, k$ (and those starting at s''_B correspond to the remaining edges), and the edges starting at s'_C correspond to the Γ_is with $i = 1, 2, \dots, k+1$ (and those starting at s''_C correspond to the remaining ones). Observe that, measured in counterclockwise order, either the angle from Γ_1 to Γ_{k+1}, or the angle from Γ_{k+1} to Γ_m is less than π. Without loss of generality, we may assume that the angle from Γ_1 to Γ_{k+1} is less than π.

First, we truncate the spherical neighborhood of s by a plane P sufficiently close to but outside s, and investigate the equilibrium points of the truncated body with respect to c. In the generic case, we have two possibilities for the graph of the truncated body K_P. If $K \cap P$ does not contain a new stable point, then the graph of K_P remains homeomorphic to A. Furthermore, if $K \cap P$ does contain a new stable point s'', then a new saddle point is created on $P \cap \partial K$, and every heteroclinic orbit on K intersecting P ends up at s (cf. Fig. 10a), whereas those not intersecting it remain the same. Finally, note also that $K \cap P$ contains a stable point if, and only if, the orthogonal projection

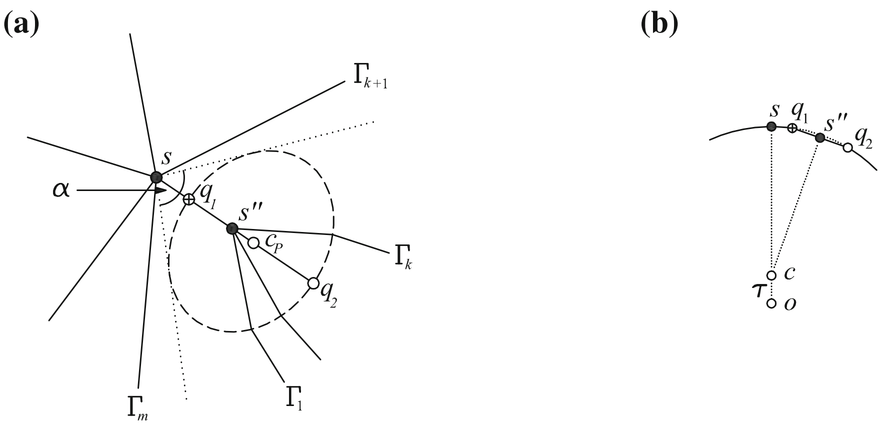

Fig. 10 **a** Truncation by the plane $P(d_{BC}, \theta, \phi)$ to create a body with graph B containing a new saddle on $P \cap \partial K$ and a sink s''. **b** An illustration for Lemma 3. The sinks s and s'' (*filled circles*) and the saddle (*circle with cross*) of (**a**) are identified

of c onto P is contained in the interior of $K \cap P$. (If the projection is contained on the boundary of this circle, it is a degenerate case corresponding to a saddle-node bifurcation.) We will find a 2-parameter family of planes such that, if the intersection circle contains the projection of o on any member, then the edges meeting the circle are either $\Gamma_1, \ldots, \Gamma_k$, or $\Gamma_1, \ldots, \Gamma_{k+1}$: see Fig. 10a.

An arbitrary plane in 3-space, and thus, in particular, the truncating plane, can be defined with three parameters. For this purpose, we use the following coordinates:

(i) d: the depth of the cut (i.e., the height of the truncated spherical cap), measured from the point of the sphere where the tangent plane is parallel to the cutting plane;
(ii) θ: the arc distance $\angle(s, o, c_p)$ of the center c_P of the intersection circle (the one created by the cutting plane on the sphere), from s, measured on $\mathbb{S}$;
(iii) ϕ: the angle of the great circle arc between c_P and s, and from some fixed great circle arc starting at s.

Up to a linear transformation, these parameters correspond to the polar coordinates of the vector pointing from the origin o to its orthogonal projection onto the truncating plane P, where the North Pole of $\mathbb{S}$ is s. Henceforth, we denote the plane by $P(d, \theta, \phi)$.

Observe that, measured in counterclockwise order, we have $\angle(\Gamma_1, \Gamma_k) < \angle(\Gamma_1, \Gamma_{k+1}) < \angle(\Gamma_0, \Gamma_{k+1}) < \angle(\Gamma_0, \Gamma_{k+2})$. Choose (cf. Fig. 10a) some angle $0 < \alpha < \pi$ satisfying

$$\angle(\Gamma_1, \Gamma_{k+1}) < \alpha < \angle(\Gamma_0, \Gamma_{k+1}). \tag{11}$$

Furthermore, for any sufficiently small, fixed value $\theta > 0$, there is a value $d_{BC} = d_{BC}(\theta, \alpha)$ independent of ϕ such that for any plane P with parameters $P(d_{BC}, \theta, \phi)$, α is the angle between the two great circle arcs on the sphere, starting at s and touching the intersection circle. Hence, by (11), there are some $\phi_B < \phi_{BC} < \phi_C$, with ϕ_B and

ϕ_C depending only on α, and $\phi_{BC} = \phi_{BC}(d)$ depending on α and d, such that

- for any $\phi \in [\phi_B, \phi_{BC}(d))$ the plane $P(d_{BC}, \theta, \phi)$ intersects Γ_i if and only if $i = 1, 2, \ldots, k$;
- the plane $P(d_{BC}, \theta, \phi_{BC}(d))$ intersects Γ_i if and only if $i = 1, 2, \ldots, k$, and it is tangent to Γ_{k+1};
- for any $\phi \in (\phi_{BC}(d), \phi_C]$ the plane $P(d_{BC}, \theta, \phi)$ intersects Γ_i if and only if $i = 1, 2, \ldots, k + 1$ (cf. Fig. 10a)). (12)

Now, consider the one-parameter family $P(d_{BC}, \theta, \phi)$, with θ fixed and depending only on $\phi \in [\phi_B, \phi_C]$. If, for any value of ϕ in this interval, the projection of c lies on $K \cap P(d_{BC}, \theta, \phi)$, then, depending on the value of ϕ, the graph of the body truncated by the plane is homeomorphic to either B or C, or in the degenerate case to BC (cf. Fig. 10a). Since we intend to use local truncations only, we would like to guarantee this property for any sufficiently small value of $\theta > 0$. Before proceeding further, we recall two lemmas from Domokos et al. (2016).

Lemma 2 *Let $r > |s - c|$ and $\delta > 0$ be arbitrary. Then there is a convex body $K' \subseteq K$ satisfying the following:*

(i) *The graph of K' is homeomorphic to A.*
(ii) *Denoting the critical point of K' corresponding to s by s', s' has a spherical cap neighborhood in $\partial K'$, of radius arbitrarily close to r.*
(iii) *Denoting the integral curve of K' corresponding to Γ_i by Γ'_i for every i, and by t_i and t'_i the unit tangent vectors of Γ_i and Γ'_i at s', respectively, we have that $|t'_i - t_i| < \delta$.*

We note that the same statement is proven in Domokos et al. (2016) for the case that s is an unstable point, and the radius of its spherical neighborhood is arbitrarily close to any given value $0 < r < |s - c|$.

Lemma 3 *Let C be the unit circle in the plane $\mathbb{R}^2$ with the origin o as its center, and let $c = (0, \tau)$, where $\tau > 0$. Let $q_1 = (\mu_1, \nu_1)$ and $q_2 = (\mu_2, \nu_2)$ be two points of C such that $\upsilon_1 > 0$.*

(i) *If $[q_1, q_2]$ is perpendicular to $[s, q_1]$, then $\lim\limits_{\mu_1 \to 0} \frac{\mu_2}{\mu_1} = \frac{2\tau}{1-\tau}$.*
(ii) *If the angle between $[q_1, q_2]$ and $[c, q_1]$ is $\frac{\pi}{2} - C'\mu_1$ for some constant C' independent of μ_1, then $\lim\limits_{\mu_1 \to 0} \frac{\mu_2}{\mu_1} = \frac{2\tau}{1-\tau} + 2C'$.*

Now, consider a plane $P = P(d_{BC}, \theta, \phi)$ with an arbitrary value of ϕ (cf. Fig. 10a), and let the closest and the farthest points of the circle $\bar{C} = P \cap \partial K$ from the segment $[o, s]$ be denoted by q_2 and q_1, respectively. For convenience, we imagine, for the moment, the plane containing $q_1 = (\mu_1, \nu_1)$, $q_2 = (\mu_2, \nu_2)$, and $c = (0, \tau)$ as $\mathbb{R}^2$ in Lemma 3: Fig. 10b.

For any sufficiently small $\theta > 0$, we require that the orthogonal projection of c on P lie in the interior of the segment $[q_1, q_2]$. Since $\angle(q_1, q_2, c) < \frac{\pi}{2}$, this property holds if and only if $\angle(q_2, q_1, c) < \frac{\pi}{2}$ for any sufficiently small $\theta > 0$. Recall that d_{BC} is defined by the fact that the angle between the two tangent lines of $\bar{C}$, passing through p, is equal to α. Let $\bar{C}^s$, q_1^s, and q_2^s denote the central projections of $\bar{C}$, q_1, and q_2, respectively, onto the tangent plane of K at s. Then, as $\theta \to 0$, the limit of the angle between the two tangent lines of $\bar{C}_s$, passing through s, is equal to α. Thus, an elementary computation yields that, as $\theta \to 0$, the limit of the ratio of the x-coordinate of q_2^s to that of q_1^s is equal to $\frac{1+\sin\frac{\alpha}{2}}{1-\sin\frac{\alpha}{2}}$, implying that the same holds for $\lim_{\theta\to 0}\frac{\mu_2}{\mu_1}$.

We conclude that our requirement that the orthogonal projection of c on P lies inside $[q_1, q_2]$ for any sufficiently small $\theta > 0$ is satisfied if $\frac{2\tau}{1-\tau} < \frac{1+\sin(\alpha/2)}{1-\sin(\alpha/2)}$, but not if $\frac{2\tau}{1-\tau} > \frac{1+\sin(\alpha/2)}{1-\sin(\alpha/2)}$. To guarantee the former, we apply Lemma 3, and choose $\delta > 0$ sufficiently small, i.e., such that for the truncated body K' and heteroclinic orbits Γ_i, the inequalities (11) remain true with the same value of α. Let c' be the center of mass of K' and o' be the center of the spherical neighborhood of s. Furthermore, let $\tau' = \frac{|s-c'|}{|s-o'|}$. Note that for a suitable choice of r, we have $\frac{2\tau'}{1-\tau'} > \frac{1+\sin(\alpha/2)}{1-\sin(\alpha/2)}$.

According to the previous paragraph, with a little abuse of notation, we assume that for the *original body* K, for any sufficiently small $\theta > 0$, the orthogonal projection of c on $P = P(d_{BC}, \theta, \phi)$ lies in the interior of $P \cap K$. Let $d_A = d_A(\theta, \alpha)$ denote the value of d, independent of ϕ, at which the projection of c lies on the boundary of $P \cap K$.

We have shown that, for $\phi \in [\phi_B, \phi_C]$ and θ is sufficiently small, the intersection circle $P(d_{BC}, \theta, \phi) \cap K$ contains in its interior a new stable point with respect to c. Thus, the graph of any such truncated body $\bar{K}$ is homeomorphic to either B or C, or to BC. Then, we fix a sufficiently small value of θ, and take the 2-parameter family of convex bodies $K(d, \phi)$, where $d \in [0, d_{BC}]$, and $\phi \in [\phi_B, \phi_C]$, defined as the truncation of K by the plane $P(d, \theta, \phi)$: see Fig. 11). Finally, for any value of ϕ, $K(0, \phi) = K$, which shows that (10.1) in Definition 10 is satisfied. The remaining properties in Definition 10 of a weakly suitable family follow from (12). This completes the first step of the proof.

We note that the bifurcation diagram of Fig. 9 in the geometric parameters d, ϕ used for the construction of the truncating plane and that of Fig. 8a in the unfolding parameters μ_1, μ_2 of Sect. 3 are topologically *but not differentiably* equivalent. As noted in Sect. 3, the bifurcation curves meet in a tangency in Fig. 8a; however, they meet at a nonzero angle in Fig. 9.

4.2 Annihilating the Motion of Center of Mass by an Auxiliary Truncation

In this subsection, we modify the family $K(d, \phi)$ in such a way that the center of mass of every member in the modified family remains at c. To do this, we need some additional assumptions on K.

Let L be the line passing through s and c, and let w denote the point of $L \cap \partial K$ different from s. We show that $K = K_A$ can be chosen in such a way that q is not an equilibrium point, and that it does not belong to any edge of A. First we modify the convex body K_0 in class (1, 1) in Várkonyi and Domokos (2006) to satisfy this

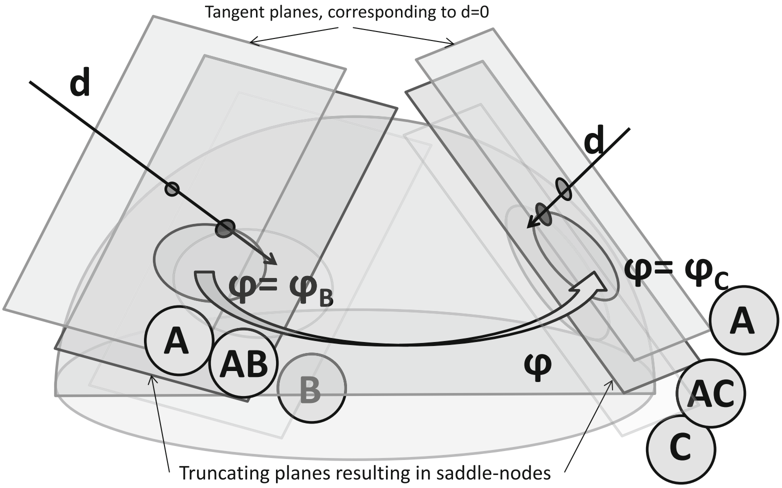

Fig. 11 The 2-parameter family of truncations used in the construction. Variation of the angle ϕ of rotation of the truncating plane results either in a saddle–saddle bifurcation, or in no bifurcation. Variation of the depth d of the truncation results in a saddle-node bifurcation; the graphs belonging to the two extremal values of ϕ are identified with capital letters

property. Since the graph of K_0 does not contain edges, we need only show that no line through the center of mass passes through more than one equilibrium point.

Since K_0 has D_4 rotational symmetry, in a suitable coordinate system, its two equilibrium points and center of mass c lie on the z-axis, and K_0 is symmetric with respect to the (x, y)-coordinate plane. Thus, all the tangent planes of K_0, parallel to the x-axis (i.e., satisfying the property that one of their translates contains the x-axis), touch K_0 at points in the (y, z)-plane. Clearly, cutting off a sufficiently small part of K_0 near the positive half of the x-axis does not change the number of equilibria nor the primary equilibrium class $\{1, 1\}$ of the body. The center of mass c' of the modified body K_0' is in the open half space $\{x < 0\}$. Hence, if the tangent plane of K_0' at some point p is perpendicular to the segment $[c', p]$, then the outer normal vectors of this plane have positive x-coordinates, implying that p is in the open half space $\{x > 0\}$. To show that any graph A can be associated with a convex body K_A satisfying this property, we observe that, by Domokes et al. (2016, Theorem 1), K_A can be obtained from K_0' by a finite sequence of local deformations.

In Domokos et al. (2016), we also showed that a neighborhood of any point of a non-isolated heteroclinic orbit, or a sink, or a source can be truncated by a sphere without changing the class of the graph of the body. Furthermore, by Domokes et al. (2016, Lemma 1), we obtain that, applying a sufficiently small truncation at w, the line connecting the modified stable point and the modified center of mass intersects this spherical surface. Thus, we may also assume that a neighborhood of w is a sphere $\mathbb{S}'$. Nevertheless, note that the center of $\mathbb{S}'$ is not necessarily on the line L. Let $c_{d,\phi}$ denote the center of mass of the *truncated* spherical cap $G(d, \phi)$ near s. To obtain a modified body $K'(d, \phi)$, we truncate K_A near q by a second plane $P'(d', \theta', \phi')$, such that the center of mass of the union of B, and the second truncated (open) spherical cap G',

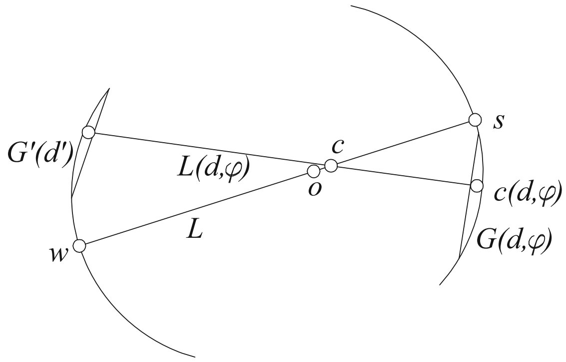

Fig. 12 The second truncation near the critical point w opposite to s; the *circular arcs* lie on the spherical caps G and G'

is c (cf. Fig. 12). Clearly, in this case the center of mass of the doubly truncated body $K'(d, \phi)$ is identical to the center of mass c of K.

Let $L(d, \phi)$ denote the line connecting c and $c(d, \phi)$. First, let d' be fixed. Then, changing θ' and ϕ', the locus of the centers of mass of G' is a part of a sphere $\mathbb{S}'_{d'}$, concentric to $\mathbb{S}'$, and the radius of this sphere depends on d' and $\mathbb{S}'$ only. Thus, if $\theta > 0$ is sufficiently small, for every line $L(d, \phi)$ and every (small) value of d' there is a unique position of G' such that its center of mass lies on $L(d, \phi)$. Let us call this cap $G' = G'(d')$. Note that the center of mass of the union of $G(d, \phi)$ and $G'(d')$ is c if and only if, the torques about c exerted by the two caps are equal. Here, the distance of the center of mass of $G'(d')$ from c is approximately $|q - c|$; that is a fixed value. Thus, by continuity, for every pair of values d, ϕ, there is at least one value of d' such that the center of mass of $G(d, \phi) \cup G'(d')$ is c. Let $G'(d, \phi)$ be the spherical cap $G'(d')$, where d' is the smallest value for which this property holds. Then, clearly, $G'(d, \phi)$ depends continuously on d and ϕ, and the 2-parameter family $K \setminus \big(G(d, \phi) \cup G'(d, \phi)\big)$ has the required properties.

5 Summary

In this paper, we showed that the secondary classification of smooth convex solids, based on the Morse–Smale complexes of their gradient vector fields, is not only complete in the sense that all combinatorially possible Morse–Smale complexes can be realized on smooth, convex bodies, but it is also complete in the more general, 'dynamical' sense that all generic transitions between Morse–Smale complexes represented by non-isomorphic abstract graphs can be realized on one-parameter families of convex bodies. Among trajectories of physical convex shape evolution processes, we find examples of such transitions, so our result implies that from a purely geometrical viewpoint, there is no restriction on these trajectories.

Theorem 3 admits only one-parameter families exhibiting one single bifurcation. However, if we only admit saddle-node bifurcations, then based on our argument in Sect. 4 we can formulate a more general claim. A codimension one, generic saddle node is either a *creation* or an *annihilation*, depending on whether the number of generic critical points increases or decreases by two. As stated before, at saddle–saddle bifurcations the number of generic critical points does not change.

To formulate the claim, we introduce

Definition 11 A generic, one-parameter family $v(\lambda)$ of gradient vector fields on the 2-sphere is called strictly monotone if it contains either only creations or only annihilations and it does not contain any saddle–saddle bifurcations.

Using this concept, we can state the following corollary to Theorem 3:

Corollary 1 *For any generic, strictly monotone, one-parameter family $v(\lambda)$ of gradient vector fields on the 2-sphere there exists a one-parameter family $K(\lambda)$ of (not necessarily smooth) convex bodies such that $\nabla r_{K(\lambda)}$ is topologically equivalent to $v(\lambda)$ for every value of λ.*

To extend this statement further, we make

Conjecture 1 Every equivalence class on the family of convex bodies, defined by the tertiary classification system, is connected. That is, for any two convex bodies K_1 and K_2 with the same topology graph A there is a one-parameter family $K(\lambda)$ of convex bodies, where $\lambda \in [0, 1]$, such that $K(0) = K_1$, $K(1) = K_2$, and the graph of $K(\lambda)$ is A for every value of λ.

Remark 1 If Conjecture 1 is true, Corollary 1 can be extended to include not only strictly monotone, but also generic families. Also, Conjecture 1 implies that any two, generic convex bodies can be connected by a generic one-parameter family of convex bodies (via the Gömböc).

It is an interesting question to ask whether any two convex bodies *in the same primary class* can be transformed into each other via a generic family of convex bodies. One essential (apparently necessary), combinatorial condition for the affirmative answer is that any two graphs in the same primary class can be transformed into each other by a series of diagonal slides. For simple 2-colored quadrangulations (i.e., which contain no multiple edges), this has been proved by Nakamoto (cf. Nakamoto 1996, and also Theorems 3 and 6 in Matsumoto and Nakamoto 2013). Remark 2 shows that this result can be extended to multigraphs in $\mathcal{Q}^2$.

Remark 2 For any $A, B \in \mathcal{Q}^2$ in the same primary class, there is a finite sequence of diagonal slides that transforms A into B up to homeomomorphism.

Proof Observe that the classes $\{1, U\}$ and $\{S, 1\}$ do not contain simple graphs, whereas all other classes do. We show that any $A \in \{S, U\}$, where $S, U \geq 2$, can be transformed into a simple graph in the same class. This, combined with Nakamoto's result, yields the assertion if $S, U \geq 2$. We note that if $S = 1$ or $U = 1$, then, using a similar technique, any graph can be transformed into the unique multigraph in which every source or sink, respectively, has degree at most two.

We carry out the transformation in two steps. First, we show that A can be transformed into a graph A' that contains no degenerate face (examples of degenerate faces

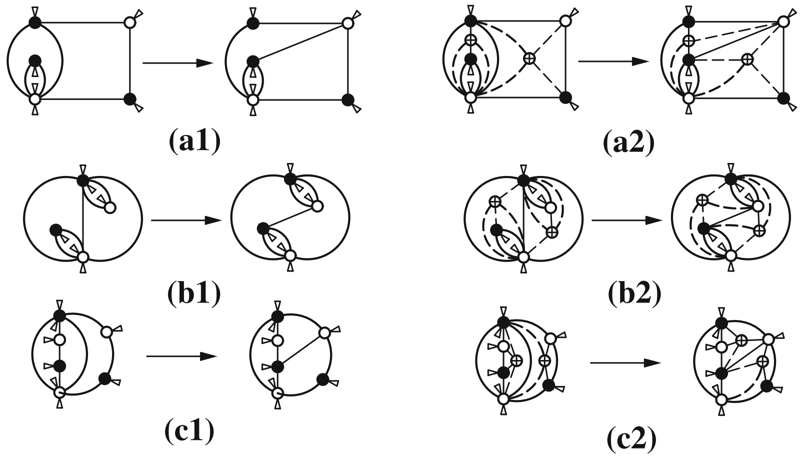

Fig. 13 Diagonal slides applied to transform a multigraph into a simple graph. The figure only illustrates the operation performed on a subgraph, *small triangles* indicate where other parts of the graph may be connected to the illustrated part. In each case degeneracy is removed by a diagonal slide. **a1**, **b1**, **c1** show the representation in $\mathcal{Q}^2$ corresponding to the proof, **a2**, **b2**, **c2** show the same operation in the $\mathcal{T}^3$ representation for easier comparison with other Figures. **a1** Removal of a degenerate face adjacent to a non-degenerate face. **b1** Removal of two degenerate faces with common edge. **c1** Removal of multiple edges on a subgraph which has only non-degenerate faces

are shown in panel b1 and c1 in Fig. 6). In the next step, we show that A' can be transformed into a graph A'' that contains no multiple edge, and thus, is simple.

Let F denote a degenerate face of A. Then, its boundary contains either a unique sink, or a unique source. If this vertex is denoted by v_i, we label F by V_i. Clearly, since $S, U \geq 2$, A contains either unlabeled or differently labeled faces. Thus, A has two faces such that they share an edge, and either exactly one of them is labeled, or they are differently labeled. Observe that if they are differently labeled, than one of them contains a unique sink, and the other one a unique source. Thus, in both cases there is a diagonal slide that transform both faces into non-degenerate ones. Figure 13a1 shows this diagonal slide if one of the faces is non-degenerate, and panel (b1) if both are non-degenerate. Hence, applying induction on the number of degenerate faces, A can be transformed into a graph A' containing only non-degenerate faces.

Now we show that A' can be transformed into a graph with no multiple edges. Choose a pair of edges E and E' of A' that start and end at the same vertices v_i and v_j. Let F_1 and F_2 be the two (non-degenerate) faces of A' adjacent to E. Observe that since these faces lie on different components of $\mathbb{S}^2$ bounded by $E \cup E'$, apart from v_i and v_j, no vertex of F_1 is connected to a vertex of F_2. Thus, applying a diagonal slide as in Fig. 13c, we reduce the number of edges connecting v_i and v_j while we do not create multiple edges between other vertices. Hence, the assertion follows by induction. □

Although our techniques do not admit the investigation of tertiary edges of $\mathcal{G}$, we also formulate

Conjecture 2 All tertiary edges of $\mathcal{G}$ are physical.

Remark 3 If Conjectures 1, 2 were true, then Remark 2 would imply that any two generic convex bodies in the same primary class can be connected by a generic family of convex bodies *without exiting* the primary class.

Remark 4 The metagraph $\mathcal{G}$ is a universal object, and there are some results concerning its complexity. In particular, the number of vertices (tertiary classes) was identified in Kápolnai et al. (2012) up to $S + U = 10$, for related work see also Cantarella (2015).

Regarding geophysical applications, we remark that in primary class {2, 2} one of the secondary classes (that of ellipsoids) appears to be dominant and the other appears to be entirely missing among natural pebble shapes. Our results show that one *could* continuously transform members of one class into members of the other class. Apparently, this process exists in natural abrasion only in one direction.

Acknowledgments This work was supported by OTKA Grant T119245 and the János Bolyai Research Scholarship of the Hungarian Academy of Sciences. Comments from an anonymous referee and Tímea Szabó are gratefully acknowledged.

References

Archdeacon, D., Hutchinson, J., Nakamoto, A., Negami, S., Ota, K.: Chromatic numbers of quadrangulations on closed surfaces. J. Graph Theory **37**, 100–114 (2001)

Arnold, V.: Ordinary Differential Equations. MIT Press, Cambridge (1998)

Bloore, F.J.: The shape of pebbles. Math. Geol. **9**, 113–122 (1977)

Brinkmann, G., Greenberg, S., Greenhill, C., McKay, B., Thomas, R., Wollan, P.: Generation of simple quadrangulations of the sphere. Discrete Math. **305**, 22–54 (2005)

Cantarella, J.: Knot Probabilities in Random Diagrams. *arXiv preprint*. arXiv:1512.05749 (2015)

Domokos, G.: Monotonicity of spatial critical points evolving under curvature driven flows. J. Nonlinear Sci. **25**, 247–275 (2015)

Domokos, G., Lángi, Z.: The robustness of equilibria on convex solids. Mathematika **60**, 237–256 (2014)

Domokos, G., Lángi, Z., Szabó, T.: A topological classification of convex solids. Geom. Dedic. **182**, 95–116 (2016)

Domokos, G., Szabó, T., Várkonyi, P., Sipos, A.: Pebbles, shapes and equilibria. Math. Geosci. **42**, 29–47 (2010)

Domokos, G., Jerolmack, D., Sipos, A.A., Török, A.: How river rocks round: resolving the shape-size paradox. PloS One **9**, e88657 (2014)

Dong, S., Bremer, P., Garland, M., Pasucci, V., Hart, J.: Spectral surface quadrangulation. ACM Trans. Graph. **25**, 1057–1066 (2006)

Edelsbrunner, H., Harer, J., Zomorodian, A.: Hierarchical Morse–Smale complexes for piecewise linear 2-manifolds. Discrete Comput. Geometry **30**, 87–107 (2003)

Firey, W.: The shape of worn stones. Mathematika **21**, 1–11 (1974)

Gross, J., Yellen, J.: Graph Theory and Its Applications. CRC Press, Boca Raton (2006)

Guckenheimer, J., Holmes, P.: Nonlinear Oscillations, Dynamical Systems and Bifurcations of Vector Fields, 1st edn. Springer, New York (1983); 7th corrected printing (2002)

Hilbert, D., Cohn-Vossen, S. (eds.): Geometry and the Imagination. AMS Chelsea Publishing, Providence (1952)

Holmes, P., Rand, D.: Bifurcations of the forced van der Pol oscillator. Q. Appl. Math. **35**, 495–509 (1978)

Illenberger, J.: Pebble shape (and size!). J. Sediment. Res. **61**, 756–767 (1991)

Jerolmack, D.: Pebbles on Mars. Science **340**, 1055–1056 (2013)

Kápolnai, R., Domokos, G., Szabó, T.: Generating spherical multiquadrangulations by restricted vertex splittings and the reducibility of equilibrium classes. Period. Polytech. Electr. Eng. **56**(1), 11–20 (2012)

Matsumoto, N., Nakamoto, A.: The number of diagonal transformations in quadrangulations on the sphere. In: Akiyama, J., Kano, M., Sakai, T. (eds.) Computational Geometry and Graphs, volume 8296 of

Lecture Notes in Computer Science, vol. 8296, pp. 110–119. Springer, Heidelberg (2013). Revised selected papers from the Thailand-Japan Joint Conference (TJJCCGG2012) held at Srinakharinwirot University, Bangkok, December 6–8, 2012

Miller, K., Szabó, T., Jerolmack, D., Domokos, G.: Quantifying the significance of abrasion and selective transport for downstream fluvial grain size evolution. J. Geophyis. Res./Earth Surf. **119**, 2412–2429 (2014)

Milnor, J. (ed.): Morse Theory. Princeton University Press, Princeton (1963)

Nakamoto, A.: Diagonal transformations in quadrangulations of surfaces. J. Graph Theory **21**(3), 289–299 (1996)

Nakamoto, A.: Generating quadrangulations of surfaces with minimum degree at least 3. J. Graph Theory **30**, 223–234 (1999)

Negami, S., Nakamoto, A.: Diagonal transformations of graphs on closed surfaces. Sci. Rep. Yokohama Nat. Univ., Sec. I **40**, 71–97 (1993)

Rayleigh, L.: The ultimate shape of pebbles, natural and artificial. Proc. R. Soc. Lond. A **181**, 107–118 (1942)

Rayleigh, L.: Pebbles, natural and artificial. Their shape under various conditions of abrasion. Proc. R. Soc. Lond. A **182**, 321–334 (1944)

Rayleigh, L.: Pebbles of regular shape and their production in experiment. Nature **154**, 161–171 (1944)

Sotomayor, J.: Generic one-parameter families of vector fields on two-dimensional manifolds. Bull. Am. Math. Soc. **74**, 722–726 (1968)

Várkonyi, P., Domokos, G.: Static equilibria of rigid bodies: dice, pebbles and the Poincaré–Hopf theorem. J. Nonlinear Sci. **16**, 255–281 (2006)

Varkonyi, P., Domokos, G.: Static equilibria of rigid bodies: dice, pebbles, and the poincare-hopf theorem. J. Nonlinear Sci. **16**(3), 255–281 (2006)

Williams, R., Grotzinger, J., Dietrich, W., Gupta, S., Sumner, D.: Martian fluvial conglomerates at Gale crater. Science **340**, 1068–1072 (2013)

Zingg, T.: Beitrag zur schotteranalyse. Schweiz Mineral Petrogr Mitt. **15**, 39–140 (1935)

Zomorodian, A. (ed.): Topology for Computing. Cambridge University Press, Cambridge (2005)